Semiconductor Physics, Quantum Electronics & Optoelectronics, 2017. V. 20, N 2. P. 185-190.
doi: https://doi.org/10.15407/spqeo20.02.185

PACS 34.20.cf, 81.05.uf

London forces in highly oriented pyrolytic graphite

L.V. Poperenko, S.G. Rozouvan, I.A. Shaykevich
Taras Shevchenko National University of Kyiv,
Department of Physics,
2, Prospect Glushkova,
03187Kyiv, Ukraine

Abstract. Surface of highly oriented pyrolytic graphite with terrace steps was studied using scanning tunneling microscopy with high spatial resolution. Spots with positive and negative charges were found in the vicinity of the steps. Values of the charges depended both on the microscope needle scan velocity and on its motion direction. The observed effect was theoretically explained with account of London forces that arise between the needle tip and the graphite surface. In this scheme, a terrace step works as a nanoscale diode for surface electric currents.

Keywords: London force, pyrolytic graphite, scanning tunneling microscopy.

Manuscript received 14.11.16; revised version received 10.04.17; accepted for publication 14.06.17; published online 18.07.17.

1. Introduction

Intermolecular forces have been known for centuries, but it's only in recent years as a result of progress in nanoscience that researchers began paying closer attention to them. As it is well-known, tiny objects on a conducting surface experience the influence of short range (van der Waals) forces, which have to be taken into account as nanodevice constructions. Three similar phenomena were subsequently shown to contribute to these "van der Waals" interactions [1]: randomly orienting dipole-dipole (or orientation) interactions, described by Keesom [2-5]; randomly orienting dipole-induced dipole (or induction) interactions, described by Debye [6, 7]; fluctuating dipole-induced dipole (or dispersion) interactions, described by London [8]. The Lifshitz theory of condensed media interaction [9] describes the short range forces based on continuum properties. The van der Waals pressure according to Lifshitz's theory can be expressed in terms of the dielectric susceptibilities of interacting phases. Hamaker developed the theory of van der Waals–London interactions between macroscopic bodies in 1937 and showed that the additivity of these interactions renders them considerably more long-range [10]. If we have objects of complicated shape and mutual position, an image method allows computing the dispersion van der Waals interaction between a neutral but polarizable atom and a perfectly conducting surface of arbitrary shape. This method has the advantage of relating the quantum problem to a well-known classical one in electrostatics [11]. Casimir force between mirrors in vacuum can now be measured with good accuracy and according to theory, when the effect of imperfect reflection of mirrors is properly taken into account [12]. A simple case of bulk metallic mirrors can be described by a plasma model to show that simple scaling laws are obtained at the limits of long and short distances. The crossover between the short and long-distance laws is quite similar to the crossover between van der Waals and Casimir–Polder forces for two atoms in vacuum. Mechanical effects in macroscopic physics and the archetype of these effects is the Casimir force between two mirrors at rest in vacuum. Casimir force, which operates at short distances, can be understood as the London interaction between the elementary excitations of both scatterers. And that is described as surface plasmons of the two bulk mirrors. At short distances, this is the van der Waals force, at large distances, the finite velocity of light becomes important (retardation effects) and the result is the Casimir force. Attractive Casimir forces were found between gold surfaces [13]. The forces were repulsive between gold and silica surfaces. The vacuum stress between closely spaced conducting surfaces, due

© 2017, V. Lashkaryov Institute of Semiconductor Physics, National Academy of Sciences of Ukraine

to the modification of the zeropoint fluctuations of the electromagnetic field in the 0.6 to 6 mm range, has been conclusively demonstrated [14]. The non-retarded Casimir–Polder interaction between a neutral but polarizable particle and a plane with a complicated topology – perfectly reacting sheet containing a circular hole was found [15]. The calculation reveals a strong dependence of the interaction on the orientation of the particle's electric dipole moment with respect to the surface.

Scanning probe microscopies (scanning tunneling microscopy (STM) and especially atomic force microscopy (AFM)) proved to be a basic tool to study nanoobjects while taking into account van der Waals forces. Significant progress has been made both in experiments and in theoretical modeling of scanning probe microscopies. See, for example, review [16] with discussions and comparison of the present status of computational modeling of scanning tunneling microscopy and scanning force microscopy in relation with their studies of surface structure and properties with atomic spatial resolution. The first stage of performing nanoscale measurements is ascertaining a good quality of the surface being studied. Metal and semiconductor crystals with lattice planes on its surface can play an important role taking into account both fabrication of nanostructures and quality of STM/AFM experiments. From the point of view, highly oriented pyrolytic graphite (HOPG) was chosen for experiments because of its close to perfect crystal lattice, which allows controlling the nanometer scale distance between interacting bodies – HOPG surface and scanning needle tip. Lattice planes on HOPG surface with sharp edges were detected applying STM in [17]. The terrace steps were characterized as crystal lattice defect though the organic impurities were mostly studied. Coiled structures with a helix pattern were studied by STM in [18]. The terraces morphology was changed by applying electrochemical reductive etching [19]. The lattice plane edges were proposed to be carbon based electrodes. The two terrace planes – edge and basal planes taken as electrodes – would exhibit different kinetics because of edge plane sites/defects [20].

The goal of this article is to study short range intermolecular forces applying atomic spatial resolution STM for lattice planes on the HOPG surface.

2. Experimental

To study the HOPG structure, we applied STM technique, which allowed us to reach an atomic spatial scale resolution. A microscope INTEGRA NT-MDT was used to conduct measurements in tunneling microscopy regime. Scanning tunneling microscopy spatial resolution reached up to 0.2 nm. A sharp needle for STM measurements was fabricated from 0.5 mm $Pt_{0.8}Ir_{0.2}$ wire by mechanically cutting its end. We performed our measurements in a regime when STM setup supported a constant tunneling current through the needle, which was completed by tuning the sample position along the vertical direction. Sample of HOPG had rectangular shape with 1 cm sides. STM measurements were performed in different places of the sample surface with a particular interest toward lattice planes edges in order to study surface effects in these spots. HOPG samples were cleaved by applying scotch tape, and the measurements were performed during the following days in order to avoid the sample surface degradation.

Examples of the HOPG surface profile studied by STM with different spatial resolution are presented in Figs 1 to 3. In Fig. 1, we can see lattice planes that form perfectly shaped terrace steps having the maximal length up to ten micrometers. The steps visible as direct straight lines separate two neighboring lattice planes that have distinct difference in brightness. The terrace steps have narrow black and white "shadows", beside which they are visible as straight and narrow bands. Fig. 2 demonstrates a high spatial resolution STM scan of a terrace step that is formed by two neighboring lattice planes. HOPG crystal lattice structure is visible on the planes. The white and black neighboring bands from Fig. 1 are marked in 3D Fig. 2 by W and B arrows that indicate sharp maximum and minimum on the edge of the step. The value of the height of the terrace step equals to 6…7 lattice parameters (~2 nm). The crystal lattice orientation of this HOPG sample was close to [101]. The terrace steps were formed during mechanical HOPG cleaving and a few terrace steps may form a group – parallel rows containing a few parallel terrace steps separated by a space interval of ten nanometers (Fig. 3). For Fig. 3 experiments, we chose terrace steps with small terrace step heights that reached 1 to 2 lattice parameters. It allowed us to register artifacts in the vicinity of the steps more noticeably. Figs 3a and 3b show the same spot of HOPG surface with parallel terrace steps, which was measured with different velocities and with different directions of needle movement along the HOPG surface.

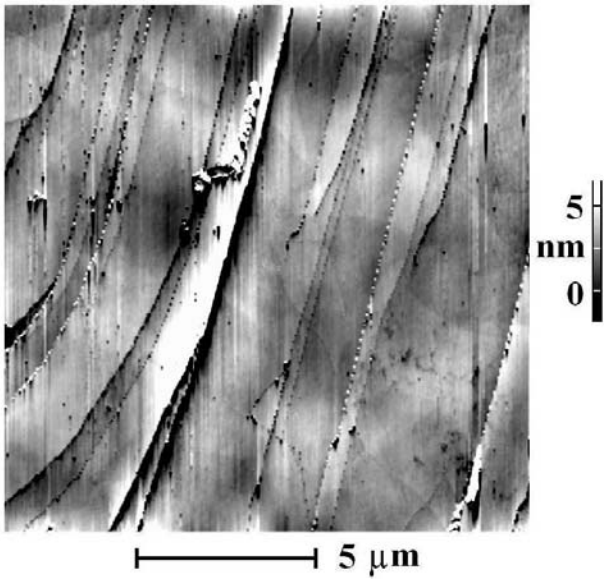

Fig. 1. STM scan of HOPG surface. Spatial resolution 60 nm.

© 2017, V. Lashkaryov Institute of Semiconductor Physics, National Academy of Sciences of Ukraine

Semiconductor Physics, Quantum Electronics & Optoelectronics, 2017. V. 20, N 2. P. 185-190.
doi: https://doi.org/10.15407/spqeo20.02.185

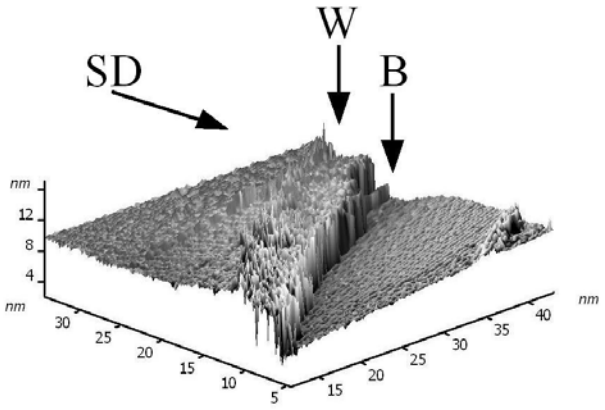

Fig. 2. STM scan of a terrace step on HOPG surface. Spatial resolution 0.2 nm. SD indicates direction of scans, W and B arrows indicate dark and white bands near the terrace step edges.

White and black areas near the terrace steps on HOPG surface are visible in Fig. 3a and have distinctly higher contrast in Fig. 3b as a result of higher scanning velocity in the latter case. The widths of the white/black bands in Fig. 3b reach 10 nm. The white/black bands are absent in Fig. 3c due to the opposite directions of the needle movement, despite the needle had the same scanning velocity as in Fig. 3b. The white spots on the two neighboring atomic planes beside of its edges indicate higher concentration of the surface charges in these areas. The electric charges contributed to the tunneling current and resulted in the large distances between the needle tip and sample surface (experimental set-up worked in the constant tunneling current regime). The dark spot similarly indicates lower surface charges in this point.

Cross sections of Fig. 3 STM scans are presented in Fig. 4. The cross sections are marked in Fig. 3 as white straight lines. The cross sections are taken in the same spot of the scanned terrace step. As we can see from plots of Fig. 4, the differences in Z coordinate near the terrace steps reach 7 nm for (a) curve and is almost unnoticeable for (c) curve (STM scan with opposite direction). For lower scan velocity ((b) curve) ΔZ is approximately 2 nm. ΔZ numbers for Fig. 4 (a) and (b) curves exceed HOPG crystal lattice parameter by almost one order of magnitude.

3. Discussion

Randomly appearing dipole on the STM needle tip induces electrical charge on the surface of HOPG. If we introduce the Green function which satisfies the expression

$$\nabla^2 G\left(\vec{r}\,',\vec{r}\,''\right) = -\delta\left(\vec{r}\,' - \vec{r}\,''\right) \qquad (1)$$

for the non-retarded interacting energy in this case between an atom with a dipole moment oriented along Z axis, and the conducting surface can be written as a simplified ratio obtained in [21]

$$U = \frac{1}{2\varepsilon_0}\left\langle d_z^2\right\rangle \nabla'_z \nabla''_z \left(G\left(\vec{r}\,',\vec{r}\,''\right) - 1/4\pi\left|\vec{r}\,' - \vec{r}\,''\right|\right)\Big|_{\vec{r}\,'=\vec{r}\,''=\vec{r}_0} . \qquad (2)$$

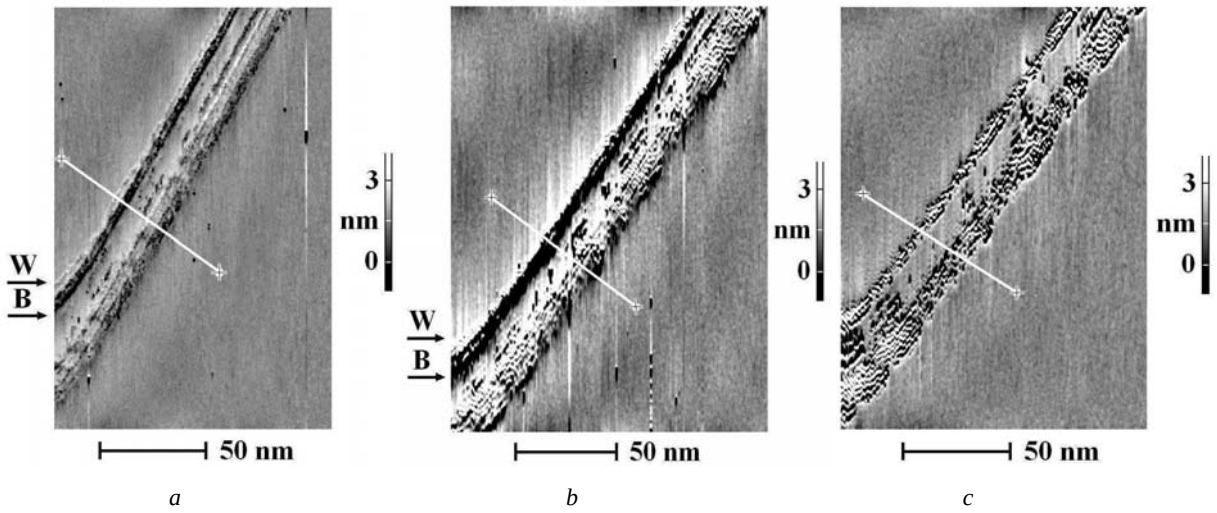

Fig. 3. STM scan of the HOPG terrace step. (a) Direction of scan from the upper part of the figure to the lower part. Velocity of scan 0.6 μm/s. Spatial resolution 0.8 nm. W and B arrows indicate dark and white bands near the terrace step edges. (b) Direction of scan from the upper part of the figure to the lower part. The velocity of scan 6 μm/s. Spatial resolution is 0.8 nm. W and B arrows indicate dark and white bands near the terrace step edges. (c) Direction of scan from the lower part of the figure to the upper part. The velocity of scan 6 μm/s. Spatial resolution is 0.8 nm.

© 2017, V. Lashkaryov Institute of Semiconductor Physics, National Academy of Sciences of Ukraine

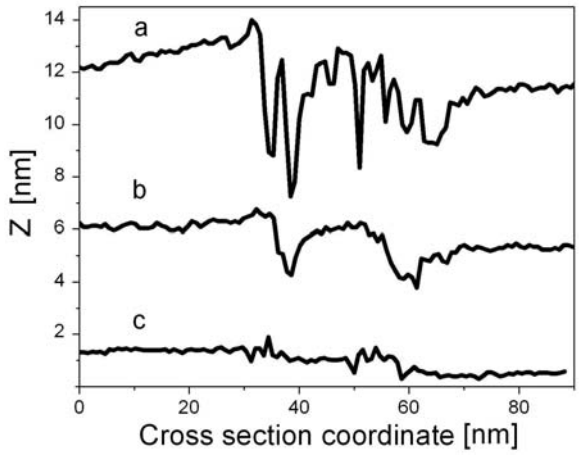

Fig. 4. Cross sections of STM scans for: a) Fig. 3b, b) Fig. 3a, c) Fig. 3c.

Here, d is a quantum operator of dipole moment that in classical approximation is equal to ql (Fig. 5), and the energy depends on its projection on Z axis. Orthogonal to the sample surface electric field E can be found with account of the image method [11], which enables to reduce the quantum mechanical problem to the related classical electrostatic one by putting additional point charges into specific places in bulk media. The electric potential in this configuration can be calculated as being induced by the original dipole and the image dipole (Fig. 4). Two dipole vectors of the both original and image dipoles are co-linear and orthogonal to the perfectly conducted sample surface in order to minimize the dipole interaction electric energy. The electric field vector in the vicinity of the sample surface is orthogonal to the surface. If applying the Coulomb law, one can calculate the electric field in an arbitrary point of the surface:

$$E(x,y)=\frac{2q}{4\pi\varepsilon_0\left(x^2+y^2+z_0^2\right)}\cdot\frac{z}{\sqrt{x^2+y^2+z_0^2}}-$$
$$-\frac{2q}{4\pi\varepsilon_0\left(x^2+y^2+(z_0+l)^2\right)}\cdot\frac{z+l}{\sqrt{x^2+y^2+(z_0+l)^2}}. \quad (3)$$

The electrical vector in (x, y) point near the surface in Eq. (3) is orthogonal to the surface and is produced by the both local surface charges and the electric dipole in the needle tip. The local electric charge density on the surface $\sigma(x, y)$ and the electric field vector $E(x, y)$ satisfy the relationship:

$$E(x,y)/2=\sigma(x,y)/2\varepsilon_0\ . \quad (4)$$

Here, only half value of the electric field $E(x, y)$ is generated by the surface charge and another half – by the dipole in the needle tip. In the image method formalism, the former part of the electric field is formed by the image dipole beneath the surface. In assumption of small l (comparing to the distance between the needle tie and the surface), we can obtain a ratio for the surface electric charge density:

$$\sigma(x,y)=\frac{d}{2\pi}\left[3z_0^2\left(x^2+y^2\right)^{-5/2}-\left(x^2+y^2+z_0^2\right)^{-3/2}\right]. \quad (5)$$

If we put an electrical dipole near a terrace step that is formed by two conducting planes, the electric field distribution cannot be found by applying the image method. First, let us take a closer look at a simple case of an electric charge near the corner of two infinite conducting semi-planes (Fig. 6a), which can be solved using the image method. In this configuration, the distribution of electric potential is generated by the real charge $+q(x_0, y_0)$ and additionally by the three mirror image charges $(-q(x_0, -y_0), -q(-x_0, y_0), +q(-x_0, -y_0))$.

The electric potential is equal to zero on the two conducting semi-planes – $x = 0$ ($y \geq 0$) and $y = 0$ ($x \geq 0$)). One real charge and three image charges form the quadruple configuration. As a result, the electric field as well as the electric charge surface density in the corner point ($x = 0$, $y = 0$ – the geometrical center of the four charges in the quadrupole) are equal to zero. If the needle tip slides along the sample surface during STM experiments, the induced surface charges on the surface also move following the moving tip. As a result, a surface current is formed.

The corner point with zero surface charge density represents a barrier or a trap, which prevents surface charge displacement from the right to the left side and from left to right. The induced surface current is equal to zero in the corner point, because as we can see from Fig. 5 calculations, surface charge density in the point is equal to zero.

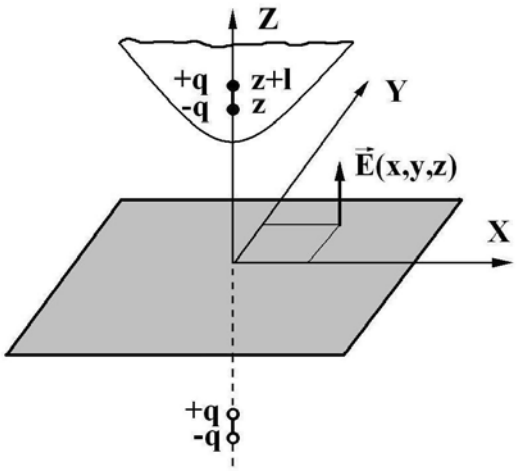

Fig. 5. A conducting needle tip with induced dipole near the conducting plane.

© 2017, V. Lashkaryov Institute of Semiconductor Physics, National Academy of Sciences of Ukraine

Semiconductor Physics, Quantum Electronics & Optoelectronics, 2017. V. 20, N 2. P. 185-190.
doi: https://doi.org/10.15407/spqeo20.02.185

A terrace step on a surface plane is a more complicated topological configuration as compared with that of the corner that is formed by two semi-infinite steps. We cannot apply the image method to obtain the electric potential distribution in this case. We tried to model the electric potential distribution in this configuration by solving numerically the Maxwell equations. The result of numerical simulation of a dipole on the STM needle tip near the terrace step on a conducting surface is presented in Fig. 6b. The calculations were performed using MEEP software in Debian Linux environment. The field distribution is shown both as equilines and gray scale surface plot. The obtained field distribution is to some extent similar to the scheme in Fig. 6a. The equilines allow us evaluating qualitatively the electric vector numbers by counting the space gap between the lines. The electric field is zero in the corner of the terrace step (similar to the scheme in Fig. 6a) and has high values near the terrace step rim. The arrow in Fig. 6b indicates possible surface charge movements through the substrate bulk material, when STM scan is performed from right to the left side. The opposite direction (from the left to the right) of surface charges movement is impossible, because the charges cannot move through the air. This scheme of surface charges movement could be a possible explanation of Fig. 3 effect, when charge is collected near the terrace step on a conducting surface, when the needle moves in one direction, and freely passes the terrace step, when the needle moves in the opposite direction. The terrace step is operating in a regime that creates a barrier (or trap) for the electric charge moving in one direction. Basically, it works as a surface nanoscale diode.

The electric current in STM experiments is formed by electrons from conduction graphite band. These electrons form ideal Fermi gas with the temperature that is below the Fermi temperature. Because of the degeneracy of the gas, we cannot register edge or defect states in the valence band of our sample similarly to [22, 23] results. If the localized surface states are registered either by spreading resistance atomic force microscopy or by Kelvin probe force microscopy, the results have to be invariant to the both scan velocity and direction.

Charges are localized near HOPG terrace steps, because the surface charges cannot move across this linear surface defect. A possible qualitative explanation can be based on a high surface curvature near terrace steps on HOPG surface and, as a result, higher values of electric field in the spots near the rims of the terrace step. The field prevents the induced surface charges from moving. In more general terms, we usually have dipole configurations of induced charge distributions in macroscopic volumes of an electric circuit, because the charges are induced there by bipolar voltage source. In nanoscale volumes, induced charges may form higher order multipole moments because of non-planar (*e.g.*, a terrace) surface topology in some spots of the surface. The induced charges in the corner of two semi-infinite conducting planes may form quadrupole configuration (quadrupole polarizability) having the zero dipole moment. This induced quadrupole forms a barrier for surface currents. The extra charges on HOPG surface are accumulated during STM needle movement and the changing local electric potential in the vicinities of terraces, which results in white/black artifact bands on STM scans. Actually, the pairs of black/white bands localized near the terrace steps indicate presence of surface nanodipoles with the vector oriented perpendicular to the terrace step direction.

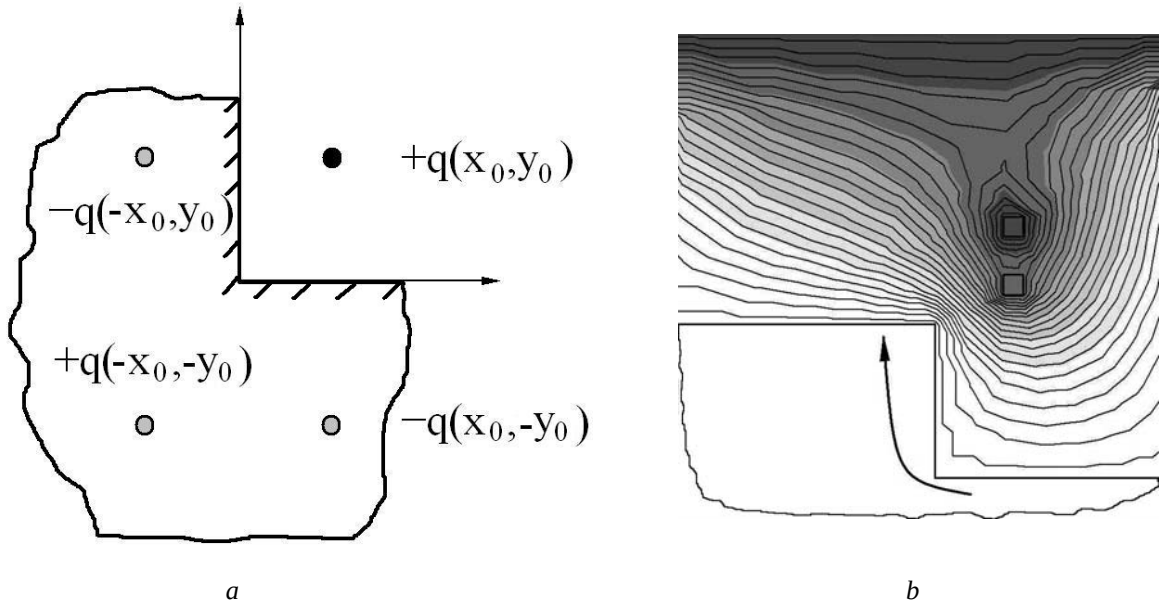

a *b*

Fig. 6. A charge near the corner of two conducting planes (a), electric potential distribution induced by a dipole near a terrace step (b).

© 2017, V. Lashkaryov Institute of Semiconductor Physics, National Academy of Sciences of Ukraine

4. Conclusions

London forces which arise between the needle tip and a conducting crystal surface during STM experiments result in induced charge in the spot beneath the needle tip. The charged spot below the needle tip on the sample surface follows the needle movement along the sample lattice plane creating a surface current. If the lattice plane has linear defects (*e.g*., terrace steps on the surface), it can result in the electric charges accumulation along the surface defect lines, when the needle moves in a specific direction. A step on a surface that forms an electric junction allows flowing surface electric current only in one direction. Practically, this effect can be used as a basic element for nanoscale diode construction. The diode dimensions could be as small as crystal lattice primitive vectors lengths. Applying another voltage polarity, one can induce a nanodipole along a sharp edge of the terrace. From pure practical point of view, it can be used as a nanoscale voltage source. This effect takes place in nanoscale volumes near the surface, because it is originated from second-order term of multipole expansion. At large distances comparing to dimensions of charge distribution the electric potential and field are dominated by the main dipole term of the expansion, and high order terms are negligible.

References

1. Van der Waals J.D. *Over de Continuiteit van den Gas- en Vloeistoftoestand (On the continuity of the gas and liquid state)*. Thesis, Leiden, 1873.
2. Keesom W.H. The second viral coefficient for rigid spherical molecules, whose mutual attraction is equivalent to that of a quadruplet placed at their centre. *Proc. R. Acad. Sci. Amsterdam*. 1915. **18**. P. 636–646.
3. Keesom W.H. The quadrupole moments of the oxygen and nitrogen molecules. *Proc. R. Acad. Sci. Amsterdam.* 1920. **23**. P. 939–942.
4. Keesom W.H. Van der Waals attractive force. *Phys. Z.* 1921. **22**. P. 129–141.
5. Keesom W.H. Van der Waals attractive force. *Phys. Z.* 1921. **22**. P. 643–644.
6. Debye P. Van der Waals Cohesive Forces. *Phys. Z.* 1920. **21**. P. 178–187.
7. Debye P. Molekularkraefte und ihre Elektrische Deutung. *Phys. Z.* 1921. **22**. P. 302–308.
8. London F.Z. Zur Theorie und Systematik der Molekularkraefte. *Phys. Z.* 1930. **63**. P. 245–279.
9. Lifshitz E.M. The theory of molecular attractive forces between solids. *Zhurnal Eksperiment. Teor Fiziki.* 1955. **29**. P. 94 (in Russian).
10. Overbeek J.T.G. Electrokinetic Phenomena. In: *Colloid Science*, vol. I. H.R. Kruyt. Elsevier, Amsterdam, 1952.
11. R. de Melo e Souza, Kort-Kamp W.J.M., Sigaud C., and Farina C. Image method in the calculation of the van der Waals force between an atom and a conducting surface. *Am. J. Phys.* 2013. **81**, No. 5. P. 366–376.
12. Genet C., Intravaia F., Lambrecht A. and Reynaud S. Electromagnetic vacuum fluctuations, Casimir and Van der Waals forces. *Annales de la Fondation Louis de Broglie.* 2004. **29**, No. 1-2. P. 331–348.
13. Bostrom M., Sernelius B., Brevik I. and Ninham B.W. Retardation turns the van der Waals attraction into a Casimir repulsion as close as 3 nm. *Phys. Rev. A.* 2012. **85**, No. 1. P. 010701.
14. Lamoreaux S.K. Demonstration of the Casimir force in the 0.6 to 6 mm range. *Phys. Rev. Lett.* 1997. **78**, No. 1. P. 5–8.
15. Eberlein C. and Zietal R. Polder interaction between a polarizable particle and a plate with a hole. *Phys. Rev. A*. 2011. **83**. P. 052514.
16. Hofer W.A., Foster A.S., Shluger A.L. Theories of scanning probe microscopes at the atomic scale. *Rev. Mod. Phys.* 2003. **75**. P. 1301.
17. McDermott M.T. and McCreery R.L. Scanning tunneling microscopy of ordered graphite and glassy carbon surfaces: Electronic control of quinone adsorption. *Langmuir.* 1994. **10**. P. 4307–4314.
18. Simonis P., Goffaux C., Thiry P.A., Biro L.P., Lambin Ph., Meunier V. STM study of a grain boundary in graphite. *Surf. Sci.* 2002. **511**. P. 319–322.
19. Kubota S., Yonezawa T., Nagahama T., and Shimada T. Change in the morphology of the terrace edges on graphite surfaces by electrochemical reduction. *Chem. Lett.* 2012. **41**, No. 2. P. 187–188.
20. Banks C.E. and Compton R.G. New electrodes for old: from carbon nanotubes to edge plane pyrolytic graphite. *Analyst.* 2006. **131**. P. 15–21.
21. Eberlein C. and Zietal R. Force on a neutral atom near conducting microstructures. *Phys. Rev. A.* 2007. **75**. P. 032516.
22. Banerjee S., Sardar M., Gayathri N., Tyagi A.K., and Raj B. Conductivity landscape of highly oriented pyrolytic graphite surfaces containing ribbons and edges. *Phys. Rev. B*. 2005. **72**. P. 075418.
23. Sommerhalter Ch., Matthes Th.W., Glatzel Th., Jager-Waldau A., and Lux-Steiner M.Ch. High-sensitivity quantitative Kelvin probe microscopy by noncontact ultra-high-vacuum atomic force microscopy. *Appl. Phys. Lett.* 1999. **75**. P. 286.

© 2017, V. Lashkaryov Institute of Semiconductor Physics, National Academy of Sciences of Ukraine